

Evaluation of fermion loops applied to the calculation of the η' mass and the nucleon scalar and electromagnetic form factors

C. Alexandrou ^{a,b}, K. Hadjiyiannakou ^{a,b}, G. Koutsou ^b, A. Ó Cais ^b and A. Strelchenko ^b

^a *Department of Physics, University of Cyprus, PoB 20537, 1678 Nicosia, Cyprus*

^b *Computation-based Science and Technology Research Center,
The Cyprus Institute, P.O. Box 27456, 1645 Nicosia, Cyprus**

(Dated: February 7, 2012)

The exact evaluation of the disconnected diagram contributions to the flavor-singlet pseudo-scalar meson mass, the nucleon σ -term and the nucleon electromagnetic form factors is carried out utilizing GPGPU technology with the NVIDIA CUDA platform. The disconnected loops are also computed using stochastic methods with several noise reduction techniques. Various dilution schemes as well as the truncated solver method are studied. We make a comparison of these stochastic techniques to the exact results and show that the number of noise vectors depends on the operator insertion in the fermion loop.

I. INTRODUCTION

An accurate estimate of disconnected contributions to flavor singlet quantities remains one of the most computational demanding problems in applying lattice Quantum Chromodynamics (QCD) to the study of hadron physics. The determination, for instance of the strange content of the nucleon, which has been extensively studied both experimentally [1–5] and theoretically, requires the evaluation of fermion loops. A nice example of an analysis that combines lattice results and chiral expansion techniques to determine the strange magnetic and electric form factors of the nucleon is presented in Refs. [6, 7]. The exact evaluation of disconnected diagrams is extremely difficult because one needs to calculate the all-to-all propagators. Furthermore, the gauge noise for some of these disconnected diagrams dominates the signal and a large number of statistics is required to reduce the error. To avoid performing all the inversions required for an exact evaluation of the all-to-all propagators, the standard approach is to use stochastic techniques with a variety of dilution schemes to estimate them. Such techniques have been applied recently in the evaluation of the η' mass, the nucleon σ -term and the electromagnetic form factors and the hadronic contribution to $g - 2$ [8–13]. The aim of this work is to evaluate a representative set of disconnected loops *exactly* and compare to the routinely used stochastic techniques in order to benchmark the various approaches. Recently one utilizes special hardware accelerators, such as graphics processors, to speed-up the inversions themselves [14, 15]. The exact evaluation is thus carried out using Graphics Cards (GPUs) to efficiently calculate the all-to-all propagator. Since the purpose of this work is to benchmark the various methods rather than produce state-of-the-art results, we use gauge configurations generated by the SESAM Collaboration [16, 17] on a relatively small lattice size of $16^3 \times 32$ in order to facilitate the exact evaluation of the fermion loops. We examine various fermion loops that enter into the evaluation of observables that have been recently studied on the lattice. These are the mass of the η' and the nucleon scalar and electromagnetic (EM) form factors.

II. LATTICE ENSEMBLE AND SIMULATION PARAMETERS

For this exploratory study we use gauge configurations generated by the SESAM/T χ L Collaboration using $N_f = 2$ Wilson fermions at $\beta = 5.6$ and hopping parameter $\kappa = 0.157$. This corresponds to a pion mass of $am_\pi = 0.3452(29)$ [17]. In order to convert to physical units we follow Ref. [17] and use the Sommer parameter, r_0 , defined through the force between two static quarks at intermediate distance [18]. The value taken from Ref. [17] is $r_0 = 0.5$ fm and at $\kappa = 0.157$ it yields for the inverse lattice spacing $a^{-1} = 2.16(3)$ GeV, giving $m_\pi = 746$ MeV. A total of 165 configurations are analyzed.

The general form of a disconnected loop is given by

$$L(x) = \text{Tr}[\Gamma G(x; x)], \quad (1)$$

*Electronic address: alexand@cyi.ac.cy (C.Alexandrou), hadjiyiannakou.kyriakos@ucy.ac.cy (K.Hadjiyiannakou), g.koutsou@cyi.ac.cy (G. Koutsou), a.s.

where for Γ we consider $\Gamma = \mathbf{1}$, γ_5 , and γ_μ and $G(x; x)$ is the Dirac propagator. The main question that we would like to address is which type of stochastic technique most efficiently reproduces the exact result and whether an optimal method exists independently of the Γ insertion in the loop. It is clearly seen from the form of Eq. (1) that, in order to evaluate quantities that involve the spatial sum of $L(x)$, one needs spatial volume more inversions than the point-to-all propagator. In this work, we evaluate exactly the all-to-all propagators for the particular set of parameters, given above. This is clearly very computational intensive and it is therefore beneficial to take advantage of graphics accelerators. We employ the QUDA library, which provides mixed precision implementations of conjugate gradient (CG) and BiCGstab solvers for the NVIDIA CUDA platform, in order to evaluate the all-to-all propagators [19]. The exact result then provides a benchmark at the level of gauge-noise for the quantities with contributions from disconnected loops. We note that GPUs are used for performing all the inversions including those for the stochastic evaluation. We would like to point out that increasing the number of configurations to reduce the gauge noise is expensive since this would require evaluating more all-to-all propagators. Therefore in this work we limit ourselves to 165 gauge configurations.

The stochastic estimate of the disconnected quark loops is performed using complex Z_2 noise for the source vectors in combination with several dilution schemes and the truncated solver method [9]. Specifically, we consider space, color and spin dilution schemes. Color (spin) dilution requires three (four) times more inversions as compared to the number with no dilution, whereas even-odd partitioning of the space doubles that number. In addition to an even-odd dilution, we have also applied a *cubic* dilution, where separate sources are placed on each vertex of an elementary 3-dimensional cube and repeated throughout the lattice, leading to an increase of a factor of 8 in the number of inversions. The truncated solver method effectively partitions the problem into a low precision and high precision space [9]. A large number of low precision inversions are carried out to achieve an approximation to the propagator with low stochastic error (but only accurate to low precision). A high precision stochastic correction is then applied using a small ensemble with the corresponding inversions carried out to high precision. The size of the stochastic ensemble of noise vectors for the low precision space and the corresponding ensemble of noise vectors for the high-precision correction is examined for the various loops. Time dilution is applied in all cases and we exploit translational invariance in order to limit the number of time slices for which the exact evaluation of the fermion loops is required.

The stochastic evaluation schemes are based on creating an ensemble of noise-vectors with the properties

$$\frac{1}{N_r} \sum_{r=1}^{N_r} \xi_\mu^a(x)_r = \langle \xi_\mu^a(x) \rangle_r \approx 0 \quad (2)$$

and

$$\frac{1}{N_r} \sum_{r=1}^{N_r} \xi_\mu^a(x)_r \xi_{\mu'}^{*a'}(x')_r = \langle \xi_\mu^a(x) \xi_{\mu'}^{*a'}(x') \rangle_r = \delta(x - x') \delta_{\mu\mu'} \delta_{aa'} \quad . \quad (3)$$

Using the above properties one has

$$\begin{aligned} \langle \phi_\mu^a(x) \xi_\nu^{*b}(y) \rangle_r &= \sum_{y'} G_{\mu\nu'}^{ab'}(x; y') \langle \xi_{\nu'}^{b'}(y') \xi_\nu^{*b}(y) \rangle_r \\ &= \sum_{y'} G_{\mu\nu'}^{ab'}(x; y') \delta(y - y') \delta_{\nu\nu'} \delta_{bb'} = G_{\mu\nu}^{ab}(x; y) \quad , \end{aligned} \quad (4)$$

where ϕ is the solution vector corresponding to a source with noise vector ξ . The above equation provides an approximation to the exact all-to-all propagator because the property of the noise vectors ξ given in Eq. (3) is exact only for an infinite ensemble of vectors. In practice, one takes a large number of noise vectors and tests the stability of results when increasing the number of vectors. In this work, we will determine how large the number of noise vectors should be, in order to obtain the exact result.

Using the stochastic estimate of the all-to-all propagator the disconnected loop is written as

$$L(\vec{x}, t_0) = \frac{1}{N_r} \sum_r \xi_\alpha^{*c}(\vec{x}, t_0)_r \Gamma_{\alpha\beta} \phi_\beta^c(\vec{x}, t_0)_r. \quad (5)$$

Given that Eq. (5) provides an estimate to the exact result the question is whether the size of the noise vector ensemble depends on the type of Γ matrix in the loop.

In the following sections we discuss the results according to the different choices of the Γ -matrices entering in the loop.

III. EVALUATION OF THE η' MASS

A general non-flavor singlet meson correlator $C_{AB}(\mathbf{p}, t)$ can be written as

$$\begin{aligned} C_{AB}(\mathbf{p}, t_f - t_i) &= \frac{1}{L^3} \sum_{\mathbf{x}_f, \mathbf{x}_i} \langle J_A(\mathbf{x}_f, t_f) J_B^\dagger(\mathbf{x}_i, t_i) \rangle \\ &= \frac{1}{L^3} \sum_{\mathbf{x}_f, \mathbf{x}_i} \langle e^{i\mathbf{p} \cdot (\mathbf{x}_f - \mathbf{x}_i)} \text{Tr} [\Gamma_A G_2(\mathbf{x}_f, t_f; \mathbf{x}_i, t_i) \Gamma_B G_1(\mathbf{x}_i, t_i; \mathbf{x}_f, t_f)] \rangle, \end{aligned} \quad (6)$$

where the interpolating field $J_A(x) = \bar{q}_1 \Gamma_A q_2$ for different quark flavors q_1 and q_2 , and $G_j(\mathbf{x}', t'; \mathbf{x}, t)$ is the propagator of quark of flavor j from space-time point (\mathbf{x}, t) to space-time point (\mathbf{x}', t') . Spin and color indices are suppressed. For flavor singlet mesons such as the η' , besides the connected part given by Eq. 6, there are disconnected contributions to the correlation function, which are given by

$$D_{AB}(\mathbf{p}, t_f - t_i) = \frac{1}{L^3} \sum_{\mathbf{x}_f, \mathbf{x}_i} \langle \text{Tr} [e^{i\mathbf{p} \cdot \mathbf{x}_f} \Gamma_A G_2(\mathbf{x}_f, t_f; \mathbf{x}_f, t_f)] \text{Tr} [e^{-i\mathbf{p} \cdot \mathbf{x}_i} \Gamma_B G_1(\mathbf{x}_i, t_i; \mathbf{x}_i, t_i)] \rangle. \quad (7)$$

Smearing is routinely used to decrease overlap with excited states. In this work, in addition to local, we consider Gaussian smeared quark fields [20, 21] for the construction of the interpolating fields:

$$\begin{aligned} q_{\text{smear}}^a(t, \mathbf{x}) &= \sum_{\mathbf{y}} F^{ab}(\mathbf{x}, \mathbf{y}; U(t)) q^b(t, \mathbf{y}), \\ F &= (\mathbb{1} + \alpha H)^n, \\ H(\mathbf{x}, \mathbf{y}; U(t)) &= \sum_{i=1}^3 [U_i(x) \delta_{x, y-i} + U_i^\dagger(x-i) \delta_{x, y+i}]. \end{aligned} \quad (8)$$

In addition, we apply APE-smearing to the gauge fields U_μ entering the hopping matrix H . All forward point-to-all propagators are computed by applying smearing taking the values of the smearing parameters $\alpha = 4.0$ and $n = 50$. These values were determined by optimizing ground state dominance for the nucleon [22]. The loops are computed without smearing throughout, including those involved in the computation of the η' mass. Since the purpose of this work is to compare exact results with those using various stochastic approaches we did not repeat the evaluation of the exact loops with smearing.

For the particular case of the η' meson and since we are using an $N_f = 2$ gauge ensemble, there are no strange quark contributions. Therefore the flavor singlet pseudo-scalar meson (also denoted by η_2 in the $N_f = 2$ theory) has only contributions from the light quarks and its two-point correlator can be written as

$$C_{\eta'}(t) = C_\pi(t) - 2D(t), \quad (9)$$

where we have taken $\mathbf{p} = 0$ and dropped the flavor indices f_1 and f_2 .

For mesons on lattices with periodic boundary conditions the two-point correlation function can be written as $C(t) \sim e^{-mt} + e^{-m(T-t)}$ for t large and $t \ll T$, where T is the lattice temporal extent. We can therefore analyze the ratio of the disconnected quark loop, $D(t)$, and connected correlation function, $C_\pi(t)$, to extract the flavor-singlet pseudo-scalar meson mass:

$$\frac{D(t)}{C_\pi(t)} \xrightarrow{t \rightarrow \infty} A - B \frac{e^{-m_{\eta'} t} + e^{-m_{\eta'} (T-t)}}{e^{-m_\pi t} + e^{-m_\pi (T-t)}}, \quad (10)$$

where m_π and $m_{\eta'}$ are the masses of the π and η' mesons and A, B are additional fit parameters. The pion mass m_π can be determined separately by fitting the pion correlator to the 1% level and used in Eq. 10 leaving only 3 parameters in the fit function. Adopting this approach allows one to use independent smearing of the connected and disconnected loops.

In the case of the exact evaluation, the only source of error comes from the statistical error of the gauge ensemble, and therefore we will employ this fact to assess the results obtained using the different stochastic methods with color, spin, even-odd and cubic dilution. In addition, we compare with the truncated solver method where for the low precision inversions using BiCGstab we set the relative deviation i.e. $|Mx_i - b|/|b|$ to 10^{-2} and for the high precision we set it to 10^{-8} , where M is the Wilson Dirac operator, x_i the solution vector after i iterations and b the source vector.

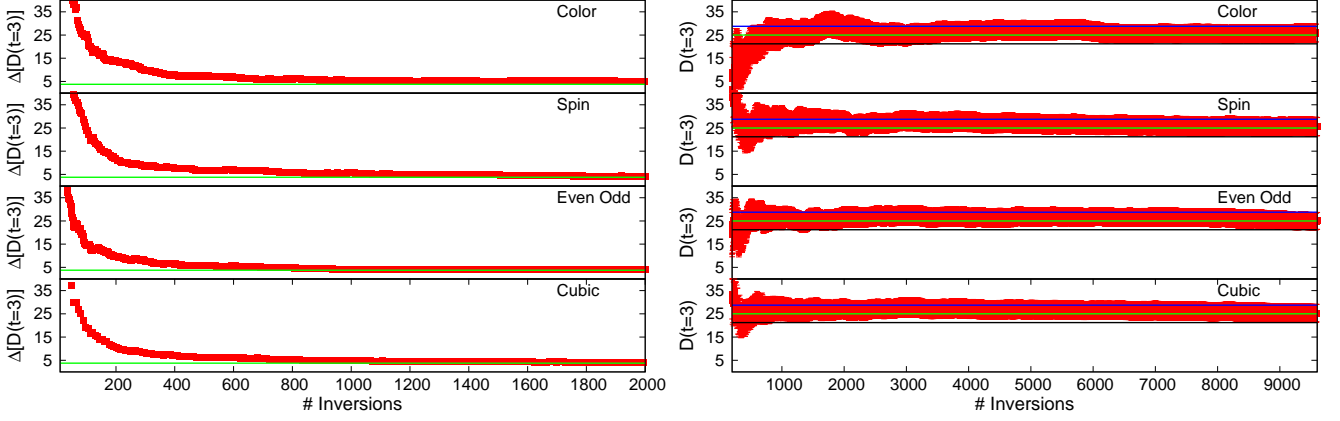


FIG. 1: Left panel: The error on the disconnected part of the η' correlator $D(t)$ at $t/a = 3$ as a function of the number of inversions. The line shows the statistical error. Right panel: The disconnected part of the η' correlator $D(t)$ at $t/a = 3$ computed stochastically as a function of the number of inversions. The lines show the mean value and error band of the exact result for $D(t)$ at the same time slice. In both graphs we show, from top to bottom, results using: color, spin, even-odd and cubic dilution.

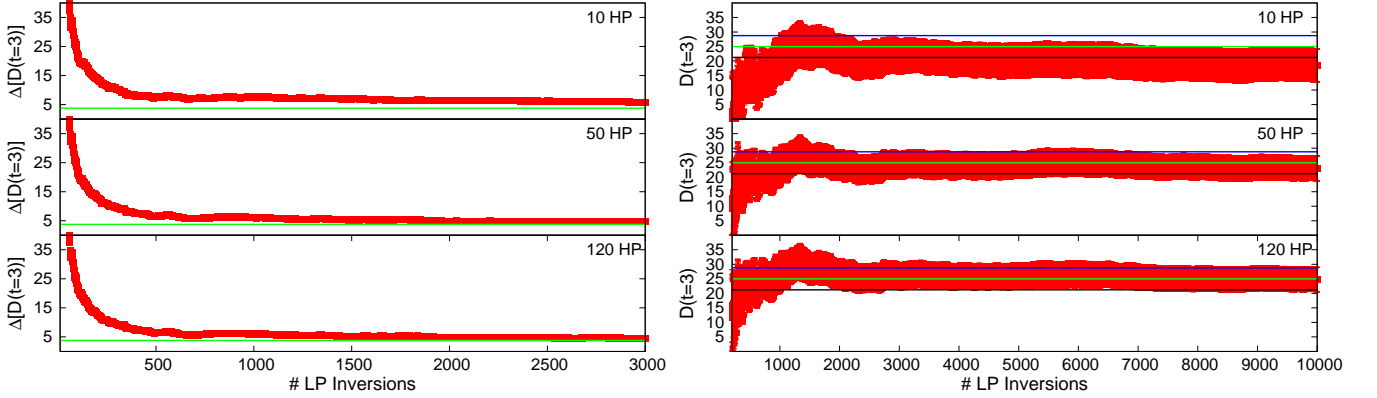


FIG. 2: In the left panel we show the error on the disconnected and on the right the disconnected part of the η' correlator $D(t)$ at $t/a = 3$ using the truncated solver method as a function of the number of low precision noise vectors for: 10 (top), 50 (middle) and 120 (bottom) high precision noise vectors. The lines show the mean value and error band of the exact result for $D(t)$ at the same time slice.

In Fig. 1 we show results for the disconnected contributions $D(t)$ at $t/a = 3$ as a function of the number of stochastic inversions using color, spin, even-odd and cubic dilution. In our case the exact result is known and, since all results are computed on the same gauge configurations, the stochastic evaluation should coincide with the result obtained from the exact evaluation of the all-to-all propagators in the limit of large enough noise vectors. Therefore, for the test case examined in this work, we show not only the error in the stochastic evaluation but also the mean value, which should coincide with that of the exact evaluation. Using a different set of gauge configurations will only reproduce the result within the statistical error and therefore in practice one requires that the error obtained in the stochastic evaluation converges to the gauge error [9]. As can be seen in Fig. 1, the stochastic error remains almost unchanged after about 600-800 inversions for the four dilution schemes used. The stochastic approach reproduces the mean value of the exact result as defined on a given set of gauge configurations and shown by the error band, in the limit of a large number of noise vectors. From this comparison we also conclude that the even-odd and cubic dilution schemes behave very similarly and therefore in what follows we will show results only for even-odd dilution, which is most commonly used.

In Fig. 2 we show results for $D(t)$ at the same time slice, namely $t/a = 3$ as used for the results in Fig. 1, but this time obtained with the truncated solver method. We display results as a function of the number of low accuracy

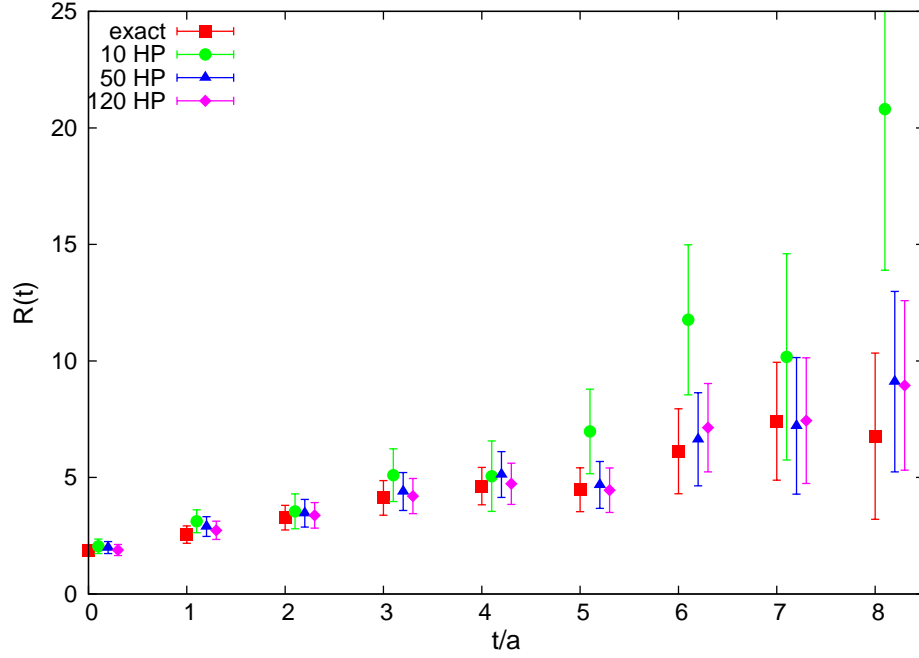


FIG. 3: The ratio $R(t) = \frac{D(t)}{C_{\pi}(t)}$ computed using the truncated solver method and the exact approach. With the filled (red) squares we show the exact calculation and with the filled (green) circles, the filled (blue) triangles and the filled (magenta) rhombus when using 10, 50 and 120 high precision noise vectors, respectively.

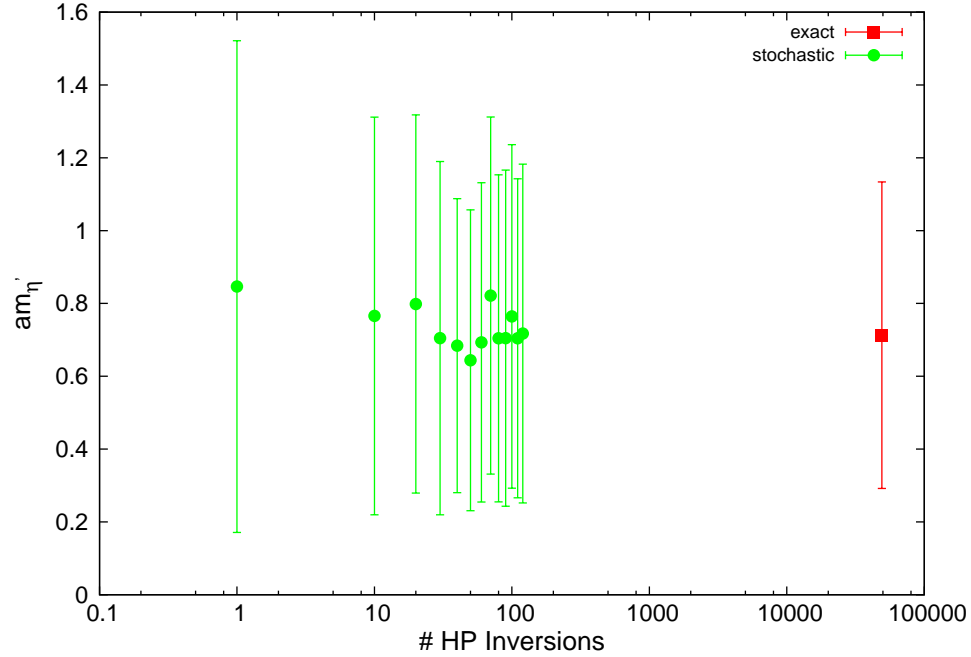


FIG. 4: The mass of η' as a function of computational cost (high precision inversions). The exact result is shown with the filled (red) squares and the results of the stochastic truncated solver method with the filled (green) circles as a function of the number of high precision vectors.

inversions increasing consecutively the number of high precision noise vectors. Since the low precision is set to relative precision 10^{-2} we only need about 10 BiCGStab iterations as compared to about 150 iterations for the high precision.

As the number of HP vectors increases the stochastic error converges to the statistical one faster. However, for 10 HP vectors, although the stochastic noise converges, the mean value remains smaller than the exact result. Therefore, one has to increase the HP vectors until also the mean value stabilizes. As can be seen, for 50 HP vectors the mean value and the error have converged when the number of low precision vectors is above about 2500 i.e. when the number of high precision noise vectors is a few percentage the number of low precision vectors. This corresponds to a cost of about 215 HP inversions as compared to about 600 for the other stochastic methods. Therefore, the truncated solver method is by far the most efficient in reproducing the exact result for the case of the loops with a γ_5 insertion.

Having established the preferred stochastic method for the evaluation of the disconnected part we turn to the determination of the η' mass in this $N_f = 2$ theory. Given that m_π is determined to the 1% level it is clear that the gauge noise, due to the disconnected loops, is large.

In Fig. 3 we compare the exact result for the ratio of disconnected to connected to the results obtained using the truncated solver method. As already mentioned, the ratio method allows us to use different smearing for the disconnected and connected. We have therefore considered smeared interpolating fields for the connected parts. As can be seen, the stochastic results converge when 50 high precision noise vectors are used. Fitting the ratio $R(t)$ from $t = 2a$ until $t = 8a$ we extract the mass of the η' shown in Fig. 4. As can be seen, increasing the number of high precision noise vectors above 50 leaves the error and mean value unchanged. Therefore the truncated solver method reproduces with low cost the exact result. This enables computation of the loop at all time slices unlike in the case of the exact result where we limit ourselves to 8 time slices. The value we extract for the mass of the η' is $am_{\eta'} = 0.54(10)$ or $m_{\eta'} = 1.17(22)$ GeV slightly higher than the value estimated by the SESAM collaboration using these configurations [23]. Recently, the mass of the η_2 meson was studied using $N_f = 2$ twisted mass fermions [8]. Within a pion mass range of about 500 MeV to about 300 MeV the dependence of the η_2 mass on the light quark mass was shown to be mild and extrapolating to the physical point a value of 0.865(65)(65) GeV was obtained. Our value is thus in reasonable agreement taking into account the higher light quark mass used in this study.

IV. NUCLEON ELECTROMAGNETIC FORM FACTORS

In order to extract the nucleon electromagnetic form factors we need to evaluate the nucleon matrix element $\langle N(p', s') | j_\mu | N(p, s) \rangle$, where $|N(p', s')\rangle$, $|N(p, s)\rangle$ are nucleon states with final momentum p' and spin s' , and initial momentum p and spin s . The nucleon electromagnetic matrix element for real or virtual photons can be decomposed in terms of the Dirac and Pauli form factors F_1 and F_2 respectively:

$$\langle N(p', s') | j^\mu | N(p, s) \rangle = \bar{u}(p', s') \left[\gamma^\mu F_1(q^2) + \frac{i\sigma^{\mu\nu} q_\nu}{2m_N} F_2(q^2) \right] u(p, s), \quad (11)$$

where $q^2 = (p' - p)^2$, m_N is the nucleon mass and $E_N(\mathbf{p})$ its energy. $F_1(0) = 1$ for the proton and zero for the neutron and $F_2(0)$ measures the anomalous magnetic moment. F_1 and F_2 are connected to the electric, G_E , and magnetic, G_M , Sachs form factors by the relations

$$\begin{aligned} G_E(q^2) &= F_1(q^2) + \frac{q^2}{(2m_N)^2} F_2(q^2) \\ G_M(q^2) &= F_1(q^2) + F_2(q^2) \end{aligned} \quad (12)$$

An interpolating field for the proton is given by

$$J(x) = \epsilon^{abc} [u^a T(x) \mathcal{C} \gamma_5 d^b(x)] u^c(x) \quad (13)$$

As described in section III, in order to increase the overlap with the nucleon state and decrease overlap with excited states we use Gaussian smeared quarks with APE smeared links.

In order to extract the nucleon matrix element of Eq. (11) we need to calculate the two-point and three-point functions in Euclidean time defined by

$$G(\mathbf{p}, t_f) = \sum_{\mathbf{x}_f} e^{-i\mathbf{x}_f \cdot \mathbf{p}} \Gamma_0^{\beta\alpha} \langle J_\alpha(\mathbf{x}_f, t_f) \bar{J}_\beta(\mathbf{0}, 0) \rangle \quad (14)$$

$$G^\mu(\Gamma_\nu, \mathbf{q}, t) = \sum_{\mathbf{x}, \mathbf{x}_f} e^{i\mathbf{x} \cdot \mathbf{q}} \Gamma_\nu^{\beta\alpha} \langle J_\alpha(\mathbf{x}_f, t_f) j^\mu(\mathbf{x}, t) \bar{J}_\beta(\mathbf{0}, 0) \rangle, \quad (15)$$

where Γ_0 and Γ_k are the projection matrices:

$$\Gamma_0 = \frac{1}{4}(\mathbb{1} + \gamma_4), \quad \Gamma_k = i\Gamma_0 \gamma_5 \gamma_k. \quad (16)$$

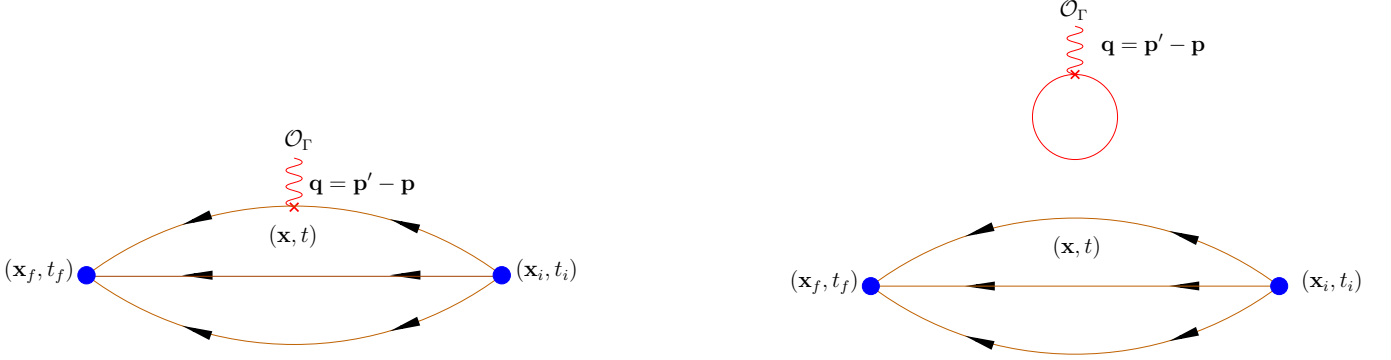


FIG. 5: Left: Connected nucleon three-point function. Right: Disconnected nucleon three-point function.

The kinematical setup that we used is illustrated in Fig. 5: The creation (source) operator at time $t_i=0$ has fixed spatial position $\mathbf{x}_i=\mathbf{0}$. The annihilation (sink) operator at a later time t_f carries momentum $\mathbf{p}'=0$. The current couples to a quark at an intermediate time t and carries the momentum \mathbf{q} . Translation invariance enforces $\mathbf{q} = -\mathbf{p}$ for our kinematics. The form factors are calculated as a function of $Q^2 = -q^2 > 0$, which is the Euclidean momentum transfer squared. Provided the Euclidean times, t and $t_f - t$ are large enough to filter the nucleon ground state, the time dependence of the Euclidean time evolution and the overlap factors cancel in the ratio

$$R^\mu(\Gamma, \mathbf{q}, t) = \frac{G^\mu(\Gamma, \mathbf{q}, t)}{G(\mathbf{0}, t_f)} \sqrt{\frac{G(\mathbf{p}, t_f - t)G(\mathbf{0}, t)G(\mathbf{0}, t_f)}{G(\mathbf{0}, t_f - t)G(\mathbf{p}, t)G(\mathbf{p}, t_f)}}, \quad (17)$$

yielding a time-independent value

$$\lim_{t_f \rightarrow \infty} \lim_{t \rightarrow \infty} R^\mu(\Gamma, \mathbf{q}, t) = \Pi^\mu(\Gamma, \mathbf{q}). \quad (18)$$

We refer to the range of t -values where this asymptotic behavior is observed within our statistical precision as the plateau range. For this study, we use the local electromagnetic current $j^\mu(x) = \bar{\psi}(x)\gamma^\mu\psi(x)$ and take the renormalization constant Z_V from Ref. [24]. We can extract the two Sachs form factors from the ratio of Eq. (17) by choosing appropriate combinations of the direction μ of the electromagnetic current and projection matrices Γ .

Inclusion of a complete set of hadronic states in the two- and three-point functions leads to the following expressions, written in Euclidean time:

$$\Pi^{\mu=i}(\Gamma_k, \mathbf{q}) = C \frac{1}{2m_N} \epsilon_{ijk} q_j G_M(Q^2) \quad (19)$$

$$\Pi^{\mu=i}(\Gamma_0, \mathbf{q}) = C \frac{q_i}{2m_N} G_E(Q^2) \quad (20)$$

$$\Pi^{\mu=0}(\Gamma_0, \mathbf{q}) = C \frac{E_N + m_N}{2m_N} G_E(Q^2), \quad (21)$$

where $C = \sqrt{\frac{2m_N^2}{E_N(E_N + m_N)}}$ is a kinematical factor connected to the normalization of the lattice states and the two-point functions entering in the ratio of Eq. (17) [25].

As schematically shown in Fig. 5, the nucleon three-point function can be written in terms of a connected and a disconnected diagram. The connected diagram can be evaluated via the standard approach of computing the sequential propagator through the sink. The polarized matrix element given in Eq. (19), from which the magnetic form factor is determined, requires an inversion for each γ_i in order that we can calculate the matrix element for all momenta \mathbf{q} in a symmetric way. For the small lattice and heavy pion mass that we have in this study, this can be done very fast. The goal of this work is the computation of the disconnected part, given by

$$\langle J_\alpha(x_f) | j^\mu(x) | \bar{J}_\beta(x_i) \rangle_{\text{Disc.}} = \frac{1}{3} \text{Tr} [\gamma^\mu G(x, x)] \times \epsilon^{abc} \epsilon^{a'b'c'} (C\gamma_5)_{\lambda\nu} (C\gamma_5)_{\lambda'\nu'} G_{\nu\nu'}^{bb'}(x_f, x_i) \left(G_{\alpha\lambda'}^{ca'}(x_f, x_i) G_{\lambda\beta}^{ac'}(x_f, x_i) - G_{\lambda\lambda'}^{aa'}(x_f, x_i) G_{\alpha\beta}^{cc'}(x_f, x_i) \right). \quad (22)$$

As shown diagrammatically, this disconnected contribution consists of the fermion loop multiplied by the nucleon two-point function. Using Eq. (15) one sees that one needs to perform the sum over the spatial coordinates of the current in the fermion loop in order to obtain the nucleon matrix element, requiring knowledge of the all-to-all propagator. Therefore the complexity lies in the evaluation of the disconnected loop.

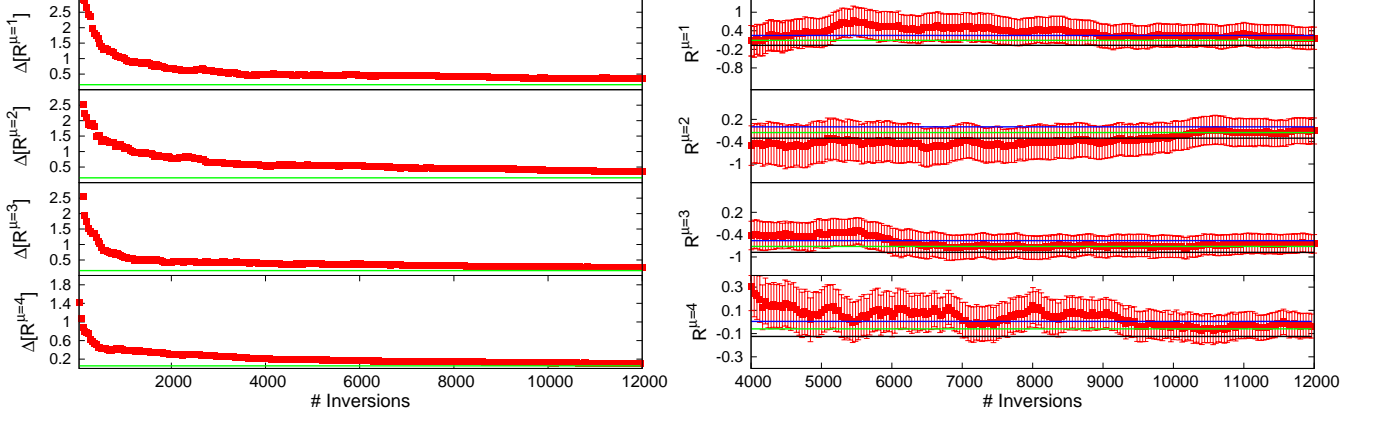


FIG. 6: On the left we show the error and on the right the ratio given in Eq. (17) for the disconnected diagram using spin dilution. The lines indicate the exact value with its error band. We show from top to bottom results: for γ_1 and $\vec{p} = (1, 0, 0)$; γ_2 and $\vec{p} = (0, 1, 0)$; γ_3 and $\vec{p} = (0, 0, 1)$; γ_4 and $\vec{p} = (1, 0, 0)$. In all cases the projection matrix Γ_0 is used and $t_f - t = 4a$.

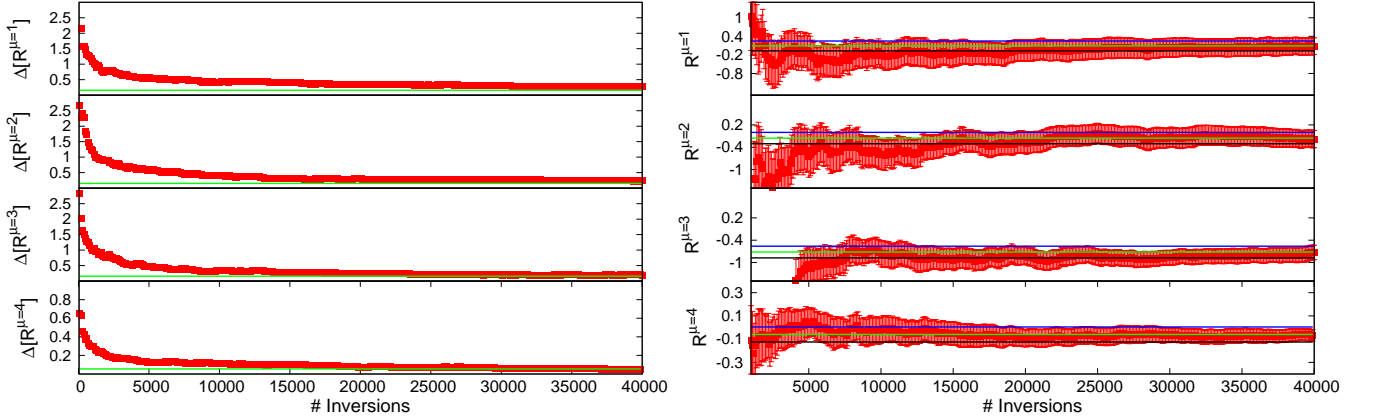


FIG. 7: On the left we show the error and on the right the ratio given in Eq. (17) for the disconnected diagram using the truncated solver method versus the number of low precision noise vectors. The number of high precision noise vectors used are 1240 for which convergence is reached. The notation is the same as that in Fig. 6.

In Fig. 6 we compare exact results for the disconnected diagram contributing to the ratio defined in Eq. (17) for various operator insertions with results obtained using spin dilution. The behavior of the other stochastic methods, i.e. using color and even-odd dilution, is similar to that of spin dilution and therefore they are not shown. As can be seen, the number of stochastic vectors needed for convergence is large. Even with about 25% the cost of the exact evaluation the results have not fully converged. Therefore these stochastic dilution schemes are not very effective for calculating the loops with a γ_μ insertion. In Fig. 7 we make a similar comparison but using the truncated solver method. We show the results as a function of the number of low precision noise vectors used. These results were obtained using of the order of 10^3 high precision noise vectors, or about 2% of the largest number of low precision vectors used. As can be seen, convergence is achieved at much lower cost since, although the number of low precision vectors used is of the same order as the number of inversions needed for the exact evaluation, the cost in the former case is much lower. Therefore the truncated solver method is by far the best choice for the fermion loops entering the evaluation of the electromagnetic form factors.

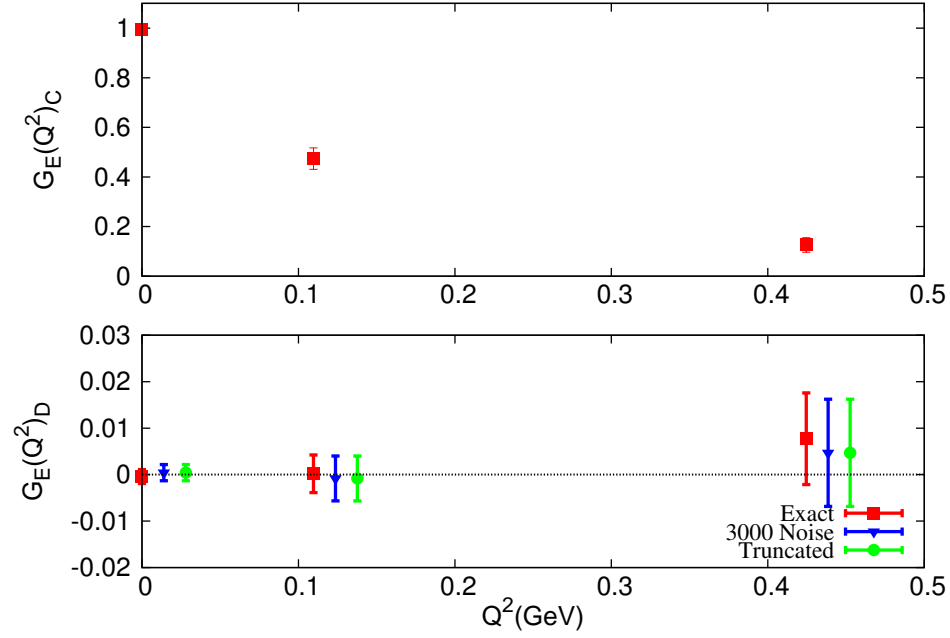


FIG. 8: Results on the connected (top) and disconnected (bottom) part for the electric form factor. The exact result is shown with the filled (red) squares. The results are compared to spin dilution for 3000 noise vectors (or 12000 inversions) shown with the filled (blue) triangles and with the truncated solver method shown with the filled (green) circles.

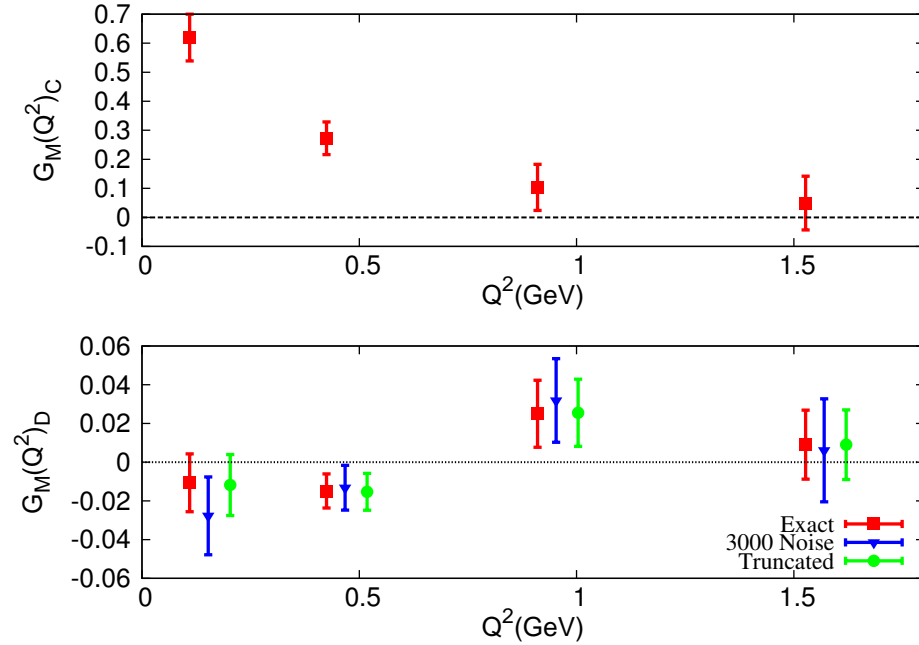


FIG. 9: Results on the connected (top) and disconnected (bottom) part of the magnetic form factor. The notation is the same as that in Fig. 8.

In Figs. 8 and 9 we show the results for the electric and magnetic form factors corresponding to the connected and disconnected contributions. As already noted, the results obtained using spin dilution have not fully converged whereas the results obtained using the truncated solver method are fully consistent with the exact evaluation. The fermion loops entering in the determination of the electromagnetic form factors are very noisy and their contribution

at this pion mass is small. A similar conclusion is reached for the nucleon strange form factors in the study of Ref. [11] where the fermion loops have similar quark mass as ours.

V. NUCLEON SCALAR FORM FACTORS

Another important quantity where fermion loops may contribute significantly is the nucleon σ -term given by

$$\sigma_l = m_l \langle N | \bar{u}u + \bar{d}d | N \rangle, \quad m_l = \frac{1}{2} (m_u + m_d). \quad (23)$$

This is proportional to the nucleon matrix element of the scalar quark density at $Q^2 = 0$. An equivalent quantity can be defined for the strange quark density. The precise knowledge of these quantities are crucial as their value affects the magnitude of the dark matter cross sections on nuclear targets. Currently the uncertainty on their values represents the largest single uncertainty affecting the cross sections relevant in various super-symmetric models. It is therefore of the utmost importance to minimize the error on the σ -terms. In this work we focus on the light quark sigma term σ_l , which is extracted from a chiral analysis of low energy pion-nucleus scattering data. However, phenomenological analyses give somewhat different results [26]. For example an earlier analysis gave $\sigma_l = 45(8)$ MeV [27], whereas a more recent one gave $\sigma_l = 64(7)$ MeV [28].

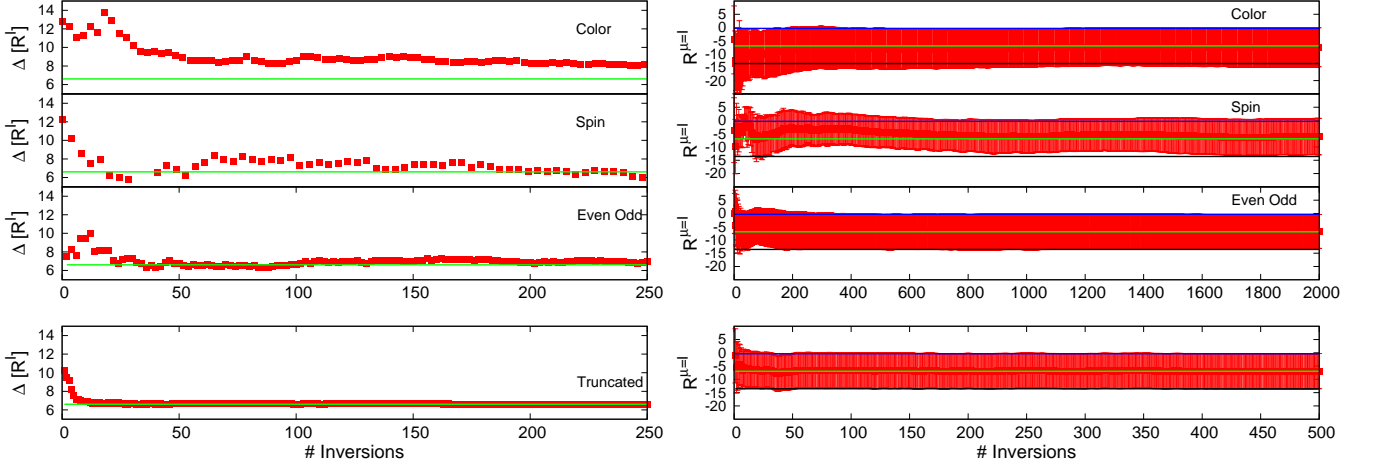


FIG. 10: Comparison of the three dilution methods (color, spin, odd-even) (top) and the truncated solver method (bottom) for the scalar current. On the left panel we show the error and on the right panel the ratio given in Eq. 17. In the case of the truncated solver method, we plot against the number of low-precision inversions, while the high precision inversions are fixed to about 2% of the maximum number of low-precision vectors used.

An indirect method to extract the nucleon σ -terms from lattice QCD without computing the disconnected diagram is to evaluate the dependence of the nucleon mass on the light and strange quark mass [22, 30–35]. However, recently stochastic methods have been applied to evaluate directly the nucleon σ -terms [9, 11]. Therefore it is interesting to compare the various approaches. In Fig. 10 we perform a comparison of the commonly used dilution schemes for the evaluation of the scalar operator. As can be seen, the convergence for this operator is much better than in the case of the electromagnetic current, presented in the previous section. Namely, for the scalar case, we converge to the exact value with as little as 500 noise vectors as compared to the case of the electromagnetic current where even using as much as 12 000 noise vectors, which corresponds to about 1/4 of the number of inversions needed for the exact evaluation, the stochastic error has not converged. Therefore it is a matter of taste which dilution scheme one employs in the evaluation of the nucleon matrix element of the scalar quark density and σ -term. The truncated solver method convergences very fast, at only a fraction of the computational cost of the other methods, and proves also here to be the most efficient. In Fig. 11 we show results on the nucleon scalar density as a function of the momentum transfer square, both for the connected and disconnected contributions. As can be seen, the exact result for the disconnected contribution is reproduced using either noise vectors with spin dilution or the truncated solver method.

In order to calculate σ_l one needs to evaluate, besides the connected and disconnected contributions, the quark mass m_l . Using the axial Ward-Takahashi identity

$$\partial^\mu A_\mu^a = 2m_q P^a, \quad (24)$$

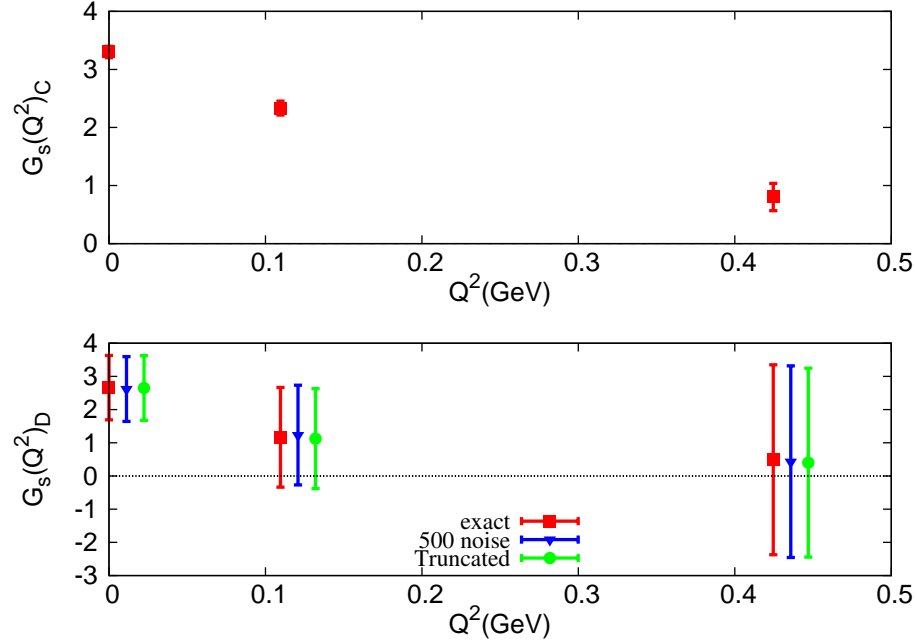


FIG. 11: The connected (top) and the disconnected (bottom) contributions of the scalar form factor. The exact result is shown with the filled (red) squares. The results are compared to spin dilution for 500 noise vectors (or 2000 inversions) shown with the filled (blue) triangles and with the truncated solver method shown with the filled (green) circles.

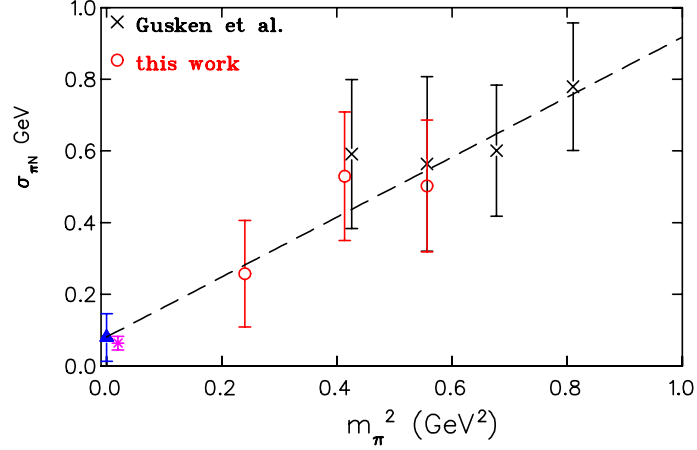


FIG. 12: The nucleon σ -term as a function of the pion mass squared. The crosses show results derived from the values of the three-point function calculated in Ref. [29], whereas the open circles are the results of this work. The line is a linear extrapolation to the chiral limit, giving the value shown by the filled triangle. The asterisk shows the value of σ_l extracted from a recent phenomenological analysis [28] with a systematic error that shows the deviation of this value from an earlier phenomenological determination given in Ref. [27].

we can extract the quark mass by taking the matrix element of Eq. (24) between a zero momentum pion state and the vacuum:

$$m_q = \frac{m_\pi \langle 0 | A_0^a | \pi^a(0) \rangle}{2 \langle 0 | P^a | \pi^a(0) \rangle} . \quad (25)$$

In order to obtain the renormalized quark mass one needs the renormalization constant for the axial-vector current Z_A and for the pseudoscalar current Z_P , whereas for the scalar density one needs Z_S , which can be taken from Ref. [24]. However, the σ -term is renormalization group invariant and therefore no renormalization is needed.

We find that the σ -term due to the connected diagram is $\sigma_l^C = 0.278(8)$ GeV and due to the disconnected $\sigma_l^D = 0.224(82)$ GeV, giving $\sigma_l = 0.50(8)$ GeV at pion mass ~ 750 MeV. This value is in agreement with an estimate made on the same ensemble in Ref. [29] if one uses their values of the connected and disconnected three-point function and the PCAC mass instead of the naive quark mass used there. In order to investigate the pion mass dependence of the σ -term, we performed the calculation using the truncated solver method for the disconnected contribution at two lighter quark masses, namely at $\kappa = 0.1575$ and $\kappa = 0.1580$ on a lattice of size $24^3 \times 48$ [17]. The values of the quark mass for this set of κ values are taken from Ref. [17]. The results are shown in Fig. 12 where we also included results from Ref. [29] but using the values of the PCAC mass given in Ref. [17]. Extrapolating linearly in the quark mass one obtains a value at the physical point that is in agreement with phenomenological estimates of this quantity, albeit with a large statistical error.

VI. CONCLUSIONS

The focus of this study is to investigate the stochastic techniques that are commonly being applied to compute fermion loops by comparing to the exact evaluation. Therefore, we perform an exact evaluation using GPUs for a relatively small lattice of $16^3 \times 32$ and $N_f = 2$ Wilson fermions corresponding to a pion mass of about 750 MeV. We consider fermion loops with the $\bar{\psi}\gamma_\mu\psi$ operator which are relevant for the electromagnetic current, flavor singlet operators relevant for the calculation of the η' mass and scalar operators relevant for the calculation of the σ -term.

Comparing color, spin and two spatial types of dilution schemes the conclusion is that they perform similarly. For the scalar operator, the convergence of these dilution schemes is much faster and one needs an order of magnitude less noise vectors as compared to the number needed when there is a γ -insertion in the loop. Comparing the aforementioned dilution schemes with the truncated solver method the conclusion is that the latter is by far the most efficient. This conclusion holds for fermion loops involving light quarks. A possible extension of this work will be the calculation of all-to-all propagators involved in other processes as for example in the evaluation of three-point diagrams. Such a study was carried out in the case of the semileptonic form factor of the D-meson [36] and it would be interesting to examine similar techniques in the case of the nucleon.

VII. ACKNOWLEDGMENT

C.A. acknowledges partial support by the Research Executive Agency (REA) of the European Union under Grant Agreement number PITN-GA-2009-238353 (ITN STRONGnet) and A. O'C. and A.S. by the Cyprus Research Foundation under grant ΙΙΡΟΣΕΑΚΥΣΗ/ΙΙΡΟΝΕ 0308/09. Computations partly utilized the Lincoln GPU cluster provided by the National Center for Supercomputing Applications. We would like to thank A. W. Thomas for very constructive comments on the nucleon σ -terms.

-
- [1] K. Aniol et al. (HAPPEX Collaboration), Phys.Rev.Lett. **96**, 022003 (2006), nucl-ex/0506010.
 - [2] D. Armstrong et al. (G0 Collaboration), Phys.Rev.Lett. **95**, 092001 (2005), nucl-ex/0506021.
 - [3] F. Maas, K. Aulenbacher, S. Baunack, L. Capozza, J. Diefenbach, et al., Phys.Rev.Lett. **94**, 152001 (2005), nucl-ex/0412030.
 - [4] F. Maas et al. (A4 Collaboration), Phys.Rev.Lett. **93**, 022002 (2004), nucl-ex/0401019.
 - [5] D. Spayde et al. (SAMPLE Collaboration), Phys.Lett. **B583**, 79 (2004), nucl-ex/0312016.
 - [6] D. B. Leinweber, S. Boinepalli, I. Cloet, A. W. Thomas, A. G. Williams, et al., Phys.Rev.Lett. **94**, 212001 (2005), hep-lat/0406002.
 - [7] D. B. Leinweber, S. Boinepalli, A. W. Thomas, P. Wang, A. G. Williams, et al., Phys.Rev.Lett. **97**, 022001 (2006), hep-lat/0601025.
 - [8] K. Jansen, C. Michael, and C. Urbach (ETM Collaboration), Eur.Phys.J. **C58**, 261 (2008), 0804.3871.
 - [9] G. S. Bali, S. Collins, and A. Schafer, Comput.Phys.Comm. **181**, 1570 (2010), 0910.3970.
 - [10] T. Doi, M. Deka, S.-J. Dong, T. Draper, K.-F. Liu, et al., Phys.Rev. **D80**, 094503 (2009), 0903.3232.
 - [11] R. Babich, R. C. Brower, M. A. Clark, G. T. Fleming, J. C. Osborn, et al. (2010), 1012.0562.
 - [12] K. Takeda et al. (JLQCD collaboration), Phys.Rev. **D83**, 114506 (2011), 1011.1964.
 - [13] X. Feng, K. Jansen, M. Petschlies, and D. B. Renner (2011), 1103.4818.
 - [14] K. Barros, R. Babich, R. Brower, M. A. Clark, and C. Rebbi, PoS **LATTICE2008**, 045 (2008), 0810.5365.
 - [15] C. Alexandrou, D. Christaras, A. O'Cais, and A. Strelchenko, PoS **LATTICE2010**, 035 (2010), 1012.5168.
 - [16] H. Hoerber et al. (TXL Collaboration, TkL Collaboration), Nucl.Phys.Proc.Suppl. **63**, 218 (1998), hep-lat/9709137.
 - [17] B. Orth, T. Lippert, and K. Schilling, Phys.Rev. **D72**, 014503 (2005), hep-lat/0503016.

- [18] R. Sommer, Nucl.Phys. **B411**, 839 (1994), hep-lat/9310022.
- [19] M. Clark, R. Babich, K. Barros, R. Brower, and C. Rebbi, Comput.Phys.Comm. **181**, 1517 (2010), 0911.3191.
- [20] C. Alexandrou, S. Gusken, F. Jegerlehner, K. Schilling, and R. Sommer, Nucl. Phys. **B414**, 815 (1994), hep-lat/9211042.
- [21] S. Gusken, Nucl. Phys. Proc. Suppl. **17**, 361 (1990).
- [22] C. Alexandrou et al. (European Twisted Mass Collaboration), Phys. Rev. **D78**, 014509 (2008), 0803.3190.
- [23] T. Struckmann et al. (TXL Collaboration, T(X)L Collaboration), Phys.Rev. **D63**, 074503 (2001), hep-lat/0010005.
- [24] D. Becirevic, B. Blossier, P. Boucaud, V. Gimenez, V. Lubicz, et al., Nucl.Phys. **B734**, 138 (2006), hep-lat/0510014.
- [25] C. Alexandrou, G. Koutsou, J. W. Negele, and A. Tsapalis, Phys. Rev. **D74**, 034508 (2006), hep-lat/0605017.
- [26] J. Giedt, A. W. Thomas, and R. D. Young, Phys.Rev.Lett. **103**, 201802 (2009), 0907.4177.
- [27] R. Koch, Z.Phys. **C15**, 161 (1982).
- [28] M. Pavan, I. Strakovsky, R. Workman, and R. Arndt, PiN Newslett. **16**, 110 (2002), hep-ph/0111066.
- [29] S. Gusken et al. (TXL Collaboration), Phys.Rev. **D59**, 054504 (1999), hep-lat/9809066.
- [30] C. Alexandrou et al. (ETM Collaboration), Phys. Rev. **D80**, 114503 (2009), 0910.2419.
- [31] R. Young and A. Thomas, Phys.Rev. **D81**, 014503 (2010), 0901.3310.
- [32] A. Walker-Loud et al., Phys.Rev. D **79** (2009), 0806.4549.
- [33] H. Ohki, H. Fukaya, S. Hashimoto, T. Kaneko, H. Matsufuru, et al., Phys.Rev. **D78**, 054502 (2008), 0806.4744.
- [34] S. Aoki et al. (PACS-CS), Phys. Rev. D **79**, 034503 (2009), 0807.1661.
- [35] S. Durr, Z. Fodor, J. Frison, T. Hemmert, C. Hoelbling, et al., PoS **LATTICE2010**, 102 (2010), 1012.1208.
- [36] R. Evans, G. Bali, and S. Collins, Phys.Rev. **D82**, 094501 (2010), 1008.3293.